DO WGANS SUCCEED BECAUSE THEY MINIMIZE THE WASSERSTEIN DISTANCE? LESSONS FROM DISCRETE GENERATORS

Anonymous authors
Paper under double-blind review

ABSTRACT

Since WGANs were first introduced, there has been considerable debate whether their success in generating realistic images can be attributed to minimizing the Wasserstein distance between the distribution of generated images and the training distribution. In this paper we present theoretical and experimental results that show that WGANs *do* minimize the Wasserstein distance but the form of the distance that is minimized depends highly on the discriminator architecture and its inductive biases. Specifically, we show that when the discriminator is convolutional, WGANs minimize the Wasserstein distance between *patches* in the generated images and the training images, not the Wasserstein distance between images. Our results leverage the advantages of *discrete* generators for which the Wasserstein distance between the generator distribution and the training distribution can be computed exactly and the minima can be characterized analytically. We present experimental results with discrete GANs that generate realistic fake images (comparable in quality to their continuous counterparts) and present evidence that they are minimizing the Wasserstein distance between real and fake patches and not the distance between real and fake images.

1 INTRODUCTION

In a seminal paper, (Arjovsky et al., 2017) showed the relationship between generative adversarial networks (GANs) and the Wasserstein distance (W_1) between two distributions. They argued that when the data lies on a low dimensional manifold, the Wasserstein distance is a more sensible optimization criterion compared to the KL divergence and showed that the Wasserstein distance can be approximately optimized using an adversarial game between two neural networks: a generator network and a critic network. The key difference between their method, Wasserstein GAN (WGAN), and previous GANs is that the critic is regularized to be 1-Lipshitz, and a great deal of subsequent research has focused on improved regularization techniques (Gulrajani et al., 2017; Miyato et al., 2018; Anil et al., 2019). WGANs have been used in many applications and can give excellent sample quality on different challenging image datasets (Radford et al., 2015; Isola et al., 2017; Brock et al., 2018; Karras et al., 2020; Sauer et al., 2022; Pan et al., 2023).

In recent years, however, the connection between the success of GANs and the Wasserstein distance has been questioned (Stanczuk et al., 2021; Fedus et al., 2018; Mallasto et al., 2019; Korotin et al., 2022; Milne & Nachman, 2022). A first criticism is the extent to which WGANs indeed minimize the Wasserstein distance. Several authors have shown that the approximating W_1 using WGANs can yield a poor approximation (Pinetz et al., 2019; Mallasto et al., 2019; Stanczuk et al., 2021; Korotin et al., 2021). A second criticism is whether minimizing the Wasserstein distance between two distributions is a sensible optimization criterion for generative models of images. Figure 1 shows a result from Mallasto et al. (2019): a model that does a much better job of minimizing an empirical estimate of the Wasserstein distance actually produces results of much lower visual quality. This had lead to an alternative view whereby ”GANs succeed because they fail to approximate the Wasserstein distance” (Stanczuk et al., 2021) and that GANs should not be seen as minimizing a loss function (Goodfellow et al., 2020; Fedus et al., 2017). Many papers had completely deserted the distribution matching approach focusing on analyzing the adversarial game and its equilibrium (Sidheekh et al., 2021; Farnia & Ozdaglar, 2020; Schäfer et al., 2019; Qin et al., 2020).

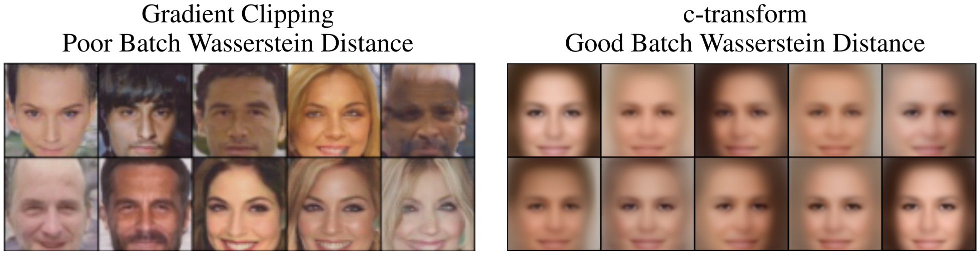
Gradient Clipping
Poor Batch Wasserstein Distance
c-transform
Good Batch Wasserstein Distance

Figure 1: When a WGAN generator is trained using gradient clipping, the approximation to Wasserstein distance is poor and a batch of generated faces have a higher Wasserstein distance to a batch from the training set compared to when the "c-transform" method is used (Mallasto et al., 2019). Nevertheless the visual quality is higher with the poor approximation.

A seemingly simple approach to answering the question of whether WGANs succeed because they minimize W_1 is to measure the Wasserstein distance between P_θ, the distribution over images that is defined by the GANs, and P_{data}, the true distribution, and to compare that distance to alternative methods that minimize $W_1(P, P_{data})$. Unfortunately, exact calculation of $W_1(P, Q)$ where P, Q are continuous distributions can only be done for a limited class of distributions. In previous works (e.g. figure 1), an empirical approximation to $W_1(P, Q)$ was used, but this approximation is known to be poor for high dimensional data such as images (Weed & Bach, 2019). Thus as long as we use continuous, nonparametric distributions for the data and the generated images, it is impossible to give a rigorous answer to the question of whether WGANs minimize W_1.

In this paper we present an alternative approach that allows us to give a rigorous answer. We leverage the advantages of *discrete* GANS. These GANS are identical to the standard GANs in which a noise vector z is passed through a neural network f_θ to generate an image. But in discrete GANs, the noise vector z is sampled uniformly from M possible fixed noise vectors and thus the generator can generate at most M possible images. Our work was motivated by our initial findings that when M is sufficiently large, discrete GANs generate images that are of comparable quality to that of standard GANs with the same architecture. Figure 2 shows images generated by a variant of FastGAN [1] that we trained as a discrete GAN with $M = 70,000$ fixed noise vectors. The results are comparable in quality to training the same architecture with continuous noise vectors and similar results are obtained with other values of M.

By using a discrete GAN we obtain the following advantages:

- We can exactly compute the Wasserstein distance between the GAN distribution P_θ and the empirical distribution P_{data}
- We can analytically characterize the optimal distribution P_θ that minimizes $W_1(P_\theta, P_{data})$ for different values of M.
- We can directly optimize $W_1(P_\theta, P_{data})$ and compare these (locally) optimal solutions to the ones found by WGANs.

In this paper we leverage these advantages of discrete GANs to provide theoretical and experimental evidence that succesful WGANs *do* minimize the Wasserstein distance but the form of the distance that is minimized depends highly on the discriminator architecture and its inductive biases. Specifically, we show that when the discriminator is convolutional, WGANs minimize the Wasserstein distance between *patches* in the generated images and the training images, not the Wasserstein distance between images.

2 EXACT COMPUTATION OF W_1 IN DISCRETE SETTING AND CHARACTERIZATION OF THE MINIMUM.

We start by reviewing the connection between Wasserstein distance and WGANs. The Wasserstein distance $W_1(P, Q)$ between two distributions is defined as:

---

[1] See appendix B.2

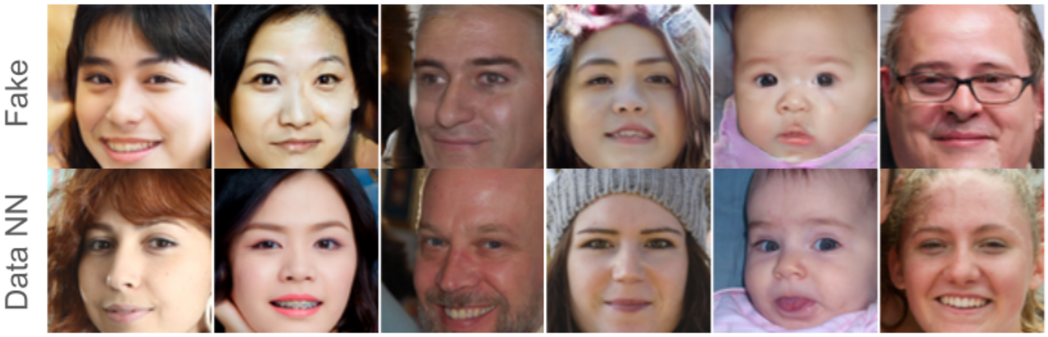

Figure 2: (top:) Images generated by a discrete version of FastGAN trained on 128x128 images from FFHQ with $M = 70,000$. Even though the generator is discrete the visual quality is high and comparable to that of the continuous generator. Similar results are obtained with different values of M. (botttom:) the closest training example to each generated image.

$$W_1(P, Q) = \inf_{\gamma \in \Pi(P,Q)} E_{x,y \sim \gamma} \|x - y\| \tag{1}$$

where $\Pi(P, Q)$ denotes the set of joint distributions whose marginal probabilities are P, Q. The connection to GANs is more evident in the dual form:

$$W_1(P, Q) = \max_{f \in F_1} E_P(f) - E_Q(f) \tag{2}$$

where F_1 is the class of 1-Lipschitz bounded functions. Thus if we denote by P the distribution over images defined by the generator and Q the training distribution, the minimization of $W_1(P, Q)$ can be performed using an adversarial game in which the the generator attempts to decrease $E_P(f) - E_Q(f)$ and the discriminator, or critic f, attempts to increase $E_P(f) - E_Q(f)$.

As mentioned in the introduction, the Wasserstein distance between arbitrary P, Q cannot be computed efficiently and in this paper we leverage the advantages of discrete distributions for which exact computation and optimization is possible.

Definition 2.1. **(Discrete distribution)** Given a set of N points $\{x_i\}_{i=1}^N$ we denote the discrete distribution defined by these points by $P_{\{x_i\}}(x) = \frac{1}{N}\delta(x - x_i)$, where δ is the Dirac delta function.

Definition 2.2. **(Discrete W_1):** Given a set of M points $\{x_i\}$ and a second set of N points $\{y_i\}$ the Wasserstein distance between the discrete distributions defined by the two sets is given by:

$$W_1(P_{\{x\}}, P_{\{y\}}) = \min_{\pi} \sum_{i,j} \pi_{ij} \|y_i - x_j\| \tag{3}$$

with π_{ij} a $M \times N$ matrix whose elements are between 0 and 1 and satisfies $\sum_i \pi_{ij} = \frac{1}{M}$,$\sum_j \pi_{ij} = \frac{1}{N}$.

Unlike the continuous case, the solution for the optimal transport matrix π can be done in polynomial time so that $W_1(P_{\{x\}}, P_{\{y\}})$ can be computed exactly. The connection to discrete GANs is described in the following definition:

Definition 2.3. **(Discrete W_1 optimization problem)**. Given a set of of N points $\{y_i\}$ the discrete W_1 optimization problem is to find a set of M points $\{x_j\}$ such that $W_1(P_{\{x\}}, P_{\{y\}})$ is minimal.

Figure 3 illustrates this problem. We approximate a training distribution with N examples (blue circles) with a generated distribution with M examples (red asterisk). The figure shows numerical solutions to this problem using an iterative algorithm that we call ”OT-Means”.

Algorithm (OT-Means). Repeat until convergence:

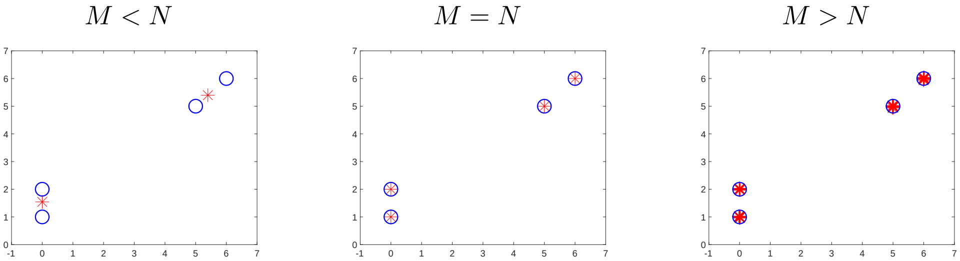

Figure 3: In the discrete Wasserstein minimization problem, we approximate a training distribution with N examples (blue circles) with a generated distribution with M examples (red asterisk). In this paper we present an algorithm (OT-means) for solving this problem and we characterize the optimal solution. Specifically, we show that when $M < N$ the optimal solution generates images that are linear combinations of training examnples, whilo for $M = N$ and $M > N$ it copies the training examples.

- Given the current estimate of the generated points $\{x_j\}$ set π to be the optimal transport matrix betwen $\{x_j\}_{j=1}^{M}$ and the training set $\{y_i\}_{i=1}^{N}$
- Given π minimize:

  $$x_j = \arg\min \sum_i \pi_{ij} \|y_i - x_j\|$$

  This minimization is the geometric median problem and can be performed using iteratively reweighted least squares (Weiszfeld, 1937).

It is easy to show that this algorithm decreases $W_1(P_{\{x\}}, P_{\{y\}})$ at each iteration.

Figure 3 shows the output of OT-means on the same toy dataset with different values of M. It can be seen that when $M < N$ the optimal solution generates samples that are linear combinations of training examples, while for $M = N$ and $M > N$ it copies the training examples. The following theorem characterizes the solutions to the problem.

Theorem 2.4. *For $M = N$ or $M > N$, $\frac{M}{N} = k$ the optimal solution to the discrete W_1 optimization problem is for the generator to copy the training examples. For$M < N$, at any local minimum of the problem, each generated sample is a linear combination of at least N/M training examples.*

Proof. (sketch) The result for $M = N$ or $M = kN$ follows from the fact that $W_1 \geq 0$ and copying the examples yields $W_1 = 0$. The result for $M < N$ follows by differentiating $W_1(P_{\{x\}}, P_{\{y\}})$ with respect to a specific x_j and setting the gradient to zero. See appendix A.1 for full proof. ☐

Given these results, we can now rigorously answer the following question: is the success of the discrete GAN shown in figure 2 due to minimizing W_1 ? This GAN was trained with $M = N = 70,000$ thus the optimal solution is to simply copy the training examples. But as can be seen, in figure 2, the discrete GAN *is not* copying the training images and when we compute the exact W_1 for this problem we see that is far from the optimal value of zero. As another example, consider the discrete GAN shown in figure 4: here $M = 10,000$ and $N = 70,000$ so at any local minimum the generated images should be a linear combination of at least 7 training images. Indeed when we run OT-means with these values of M, N we obtain images of low quality (shown in the bottom of the figure) even though the exact W_1 is better. This is reminiscent of the Mallasto et al. (2019) result in 1 but note that here we are using the exact W_1 between two discrete distributions and avoiding the intractable problem of approximating W_1 between continuous distributions.

3 THE IMPORTANCE OF THE DISCRIMINATOR ARCHITECTURE

Given the dual form of W_1 (equation 2), how do we explain the fact that WGANs do such a poor job of minimizing W_1? One possibility is that in the standard training of WGANs, the discriminator is not optimized to convergence: the common practice is to iterate a few iterations of gradient descent

Discrete FastGAN ($M = 10K$) ($W_1 \approx 1.82e04$):

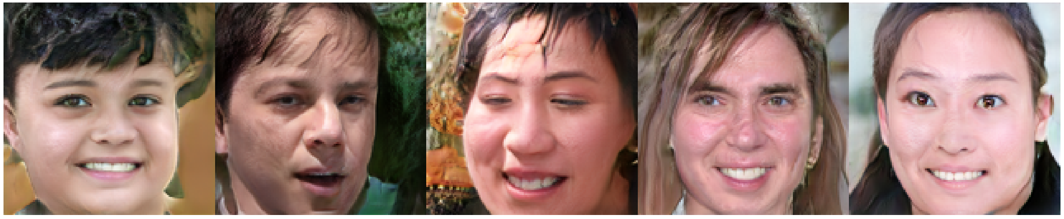

OTMeans ($M = 10K$) ($W_1 \approx 7.69e03$)):

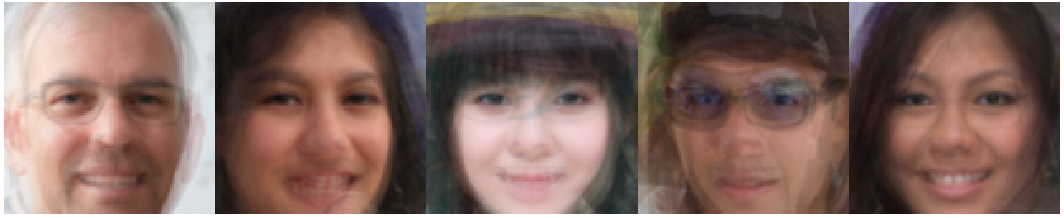

Figure 4: Top: results of discrete fastGAN with $M = 10K$ so that $M < N$. The results are still sharp and realistic. Bottom: OT means with the same M, N. This produces blurred images and yet the exact W_1 is lower.

for the generator and then a few iterations for the discriminator. Perhaps this use of iterative gradient updates precludes the WGANs from optimizing W_1 ? In this section we present evidence that this is not the case. In fact, even with iterative gradient updates, WGANs can do an excellent job of optimizing the Wasserstein distance, but the specific form of the distance that is being optimized is heavily influenced by the architecture of the discriminator.

Figures 5,6 show experiments with *fully connected discriminators*. Fully connected discriminators are interesting because they satisfy the universal approximation property Hornik et al. (1989): by using a sufficiently wide fully connected network with the gradient penalty method of WGANs, the discriminator should be able to implement any 1-Lipshitz function. In these figures, we considered three toy datasets of $N = 1000$ images: (1) white squares on a black background (2) MNIST and (3) face thumbnails (of size 64×64). We trained a discrete WGAN with a fully connected discriminator on these datasets with different values of M. The generator network was also a fully connected network and we used mini-batches of size 64. We also ran OT-means on the same data and for the same values of M. We found that for a range of values of M, *the discrete WGAN did an excellent job of minimizing* W_1.

Figure 5 shows the results for $M = 64$. Recall that given theorem 2.4, any local minimum of the loss should generate images that are linear combinations of at least 15 different training images. Indeed when we look at the results of OT-means (in the middle column) we find that the generated images are blurred, as expected. When we look at the results of the DiscreteWGAN-FC (right column) we see that they are also blurred. Unlike results that are often shown in papers that use WGANs, where the results are sharp and contain high resolution detail (e.g. figure 1), now the results are visually similar to the results of OT-means. Perhaps most convincingly, when we measure the exact W_1 between the generated images and the training set, we see that the DiscreteWGAN-FC samples achieve nearly the same W_1 as the OT-means result.

Figure 6 shows a similar pattern of results for the case $M = N$. According to theorem 2.4, in this setting the optimal W_1 is obtained when the generator simply copies the training examples. Indeed such a solution is found rapidly using OT-means. But more surprisingly, this solution is also found using the Discrete GAN: even though the generator never has direct access to the training set (only through a noisy gradient signal given by the discriminator) and is trained with mini-batches, it manages to copy the training examples and achieves a W_1 value that is close to the optimal value of zero.

Taken together, these results show that WGANs *can* do an excellent job of minimizing W_1, even with iterative gradient updates. How then do we explain the failure of W_1 minimization in successful

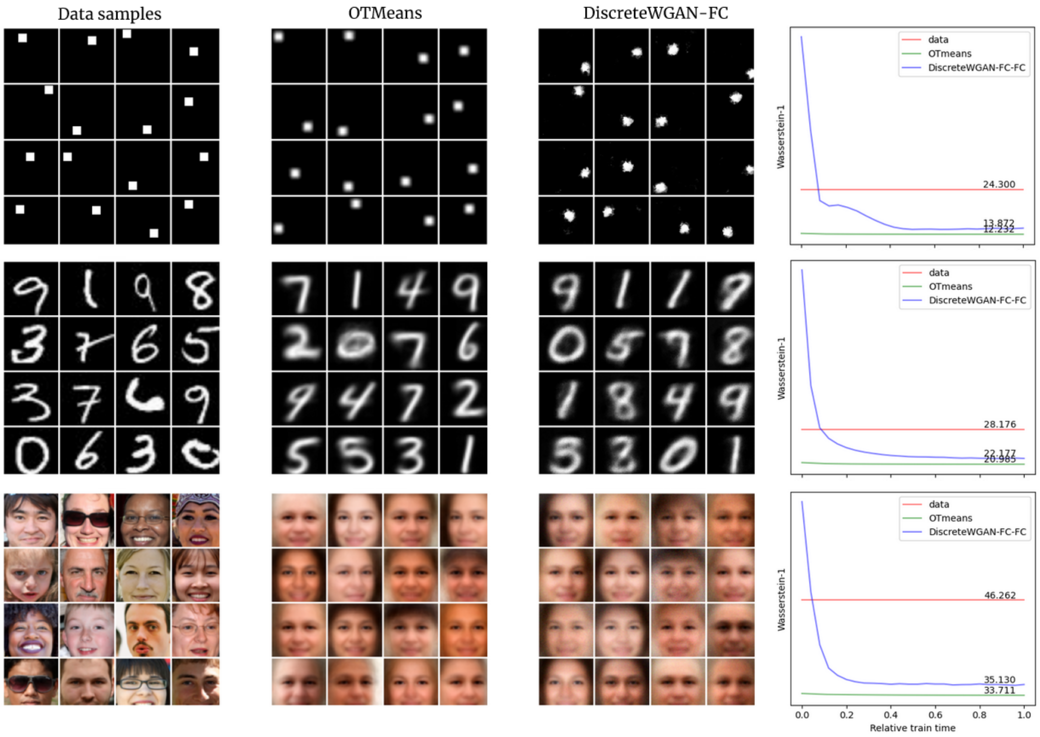

Figure 5: Using Fully connected discriminator minimizes W1 almost as well as OT means. The plots on the right compare both the optimization results and a batch of 64 training images to all train images

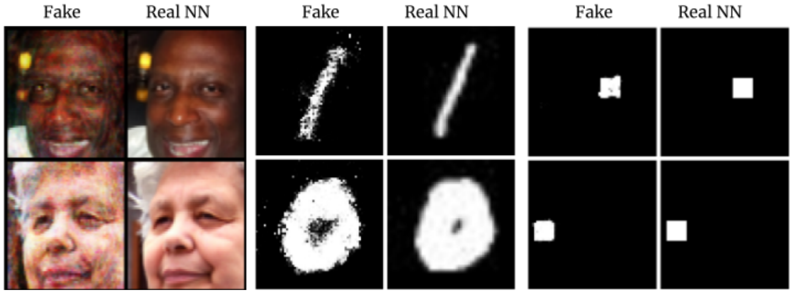

Figure 6: Using Fully connected discriminator and $M = N$ makes WGANs copy the data. Again, this is almost as good as minimizing W1 with OT-means.

WGANs such as those shown in figures 1,2? As we now show, this is due to the fact that they use *convolutional discriminators.*

3.1 CONVOLUTIONAL DISCRIMINATORS

The key assumption in the connection between WGANs and W_1 is that the discriminator can approximate any 1-Lipshitz function. But what happens if the discriminator architecture has strong inductive bias? Almost all discriminators used in practical GANs are convolutional. The following theorems shows that for such discriminators, WGANs no longer minimize W_1 between images but rather between smaller image-patches.

We start by formally defining two convolutional architectures (see detailed description in the appendix B.1).

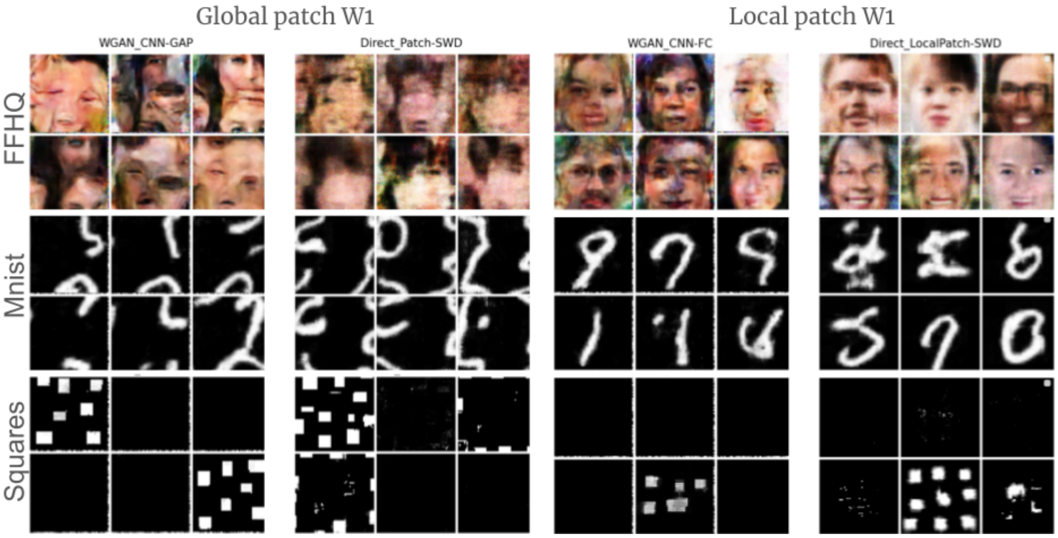

Figure 7: Using convolutional discriminators with the same generator as above learns either global patch statistics (with CNN-GAP) or local patch statistics (with CNN-FC). In all cases, the patch W1 that it finds is similar to directly optimizing the appropriate patch W1.

Definition 3.1. (**CNN-GAP**) We denote by CNN-GAP(S) a CNN in which all layers except the last two are convolutional, followed by global average pooling (GAP) and a fully connected layer. The receptive field of units in the layer before the global average pool is S.

Definition 3.2. (**CNN-FC**) We denote by CNN-FC(S) a CNN in which all layers except the last layer are convolutional followed by fully connected layer and the receptive field of units in the layer before last is S.

These two CNNs are abstractions of CNNs that are used in successful WGANs: CNN-GAP is an abstraction of the patchGAN discriminator (Isola et al., 2017) and CNN-FC is an abstraction of the DCGAN discriminator (Radford et al., 2015). More details in Appendix B.1.

Theorem 3.3. *Training a WGAN with a CNN-GAP discriminator is equivalent to minimizing* $W_1(\hat{P}_\theta, \hat{P}_{data})$ *where* $\hat{P}_\theta, \hat{P}_{data}$ *are the distribution over all* patches *of size* S *in the generated images and training images respectively.*

Proof. (sketch) For this discriminator the output can be written as a sum of discriminators over patches and by linearity of expectation $E_P(f), E_Q(f)$ can be written as a sum of expectations over patch distributions. Full proof in A.2 ☐

Theorem 3.4. *Training a WGAN with a CNN-FC discriminator is equivalent to minimizing an upper bound on* $W_1(\widehat{P_\theta^{i,j}}, \widehat{P_{data}^{i,j}})$ *where* $\widehat{P_\theta^{i,j}} \widehat{P_{data}^{i,j}}$ *are the distributions over all* patches *of size* S *in the generated images and training images respectively at location* (i, j)*. This bound holds for any location* (i, j)*.*

Proof. (sketch) For this discriminator the output can be written as a weighted sum of discriminators over patches at a specific location. By choosing the weights to be one only at one location and zero everywhere else, we obtain a bound on the Wasserstein distance between fake and generated patches at that location. Full proof in A.3. ☐

Figure 7 (1st and 3rd left columns) shows the dramatic influence of the discriminator architecture on the toy datasets that we showed in figure 5, Even though we are using exactly the same value of M (64) and exactly the same training set and generator architecture, the Discrete GANs with CNN discriminators generate completely different images compared to OTmeans (Fig. 5). While the OTmeans results (and the discreteGANs with non convolutional discriminators) look blurred and maintain global structure, the images generated by the GANs with convolutional discriminators

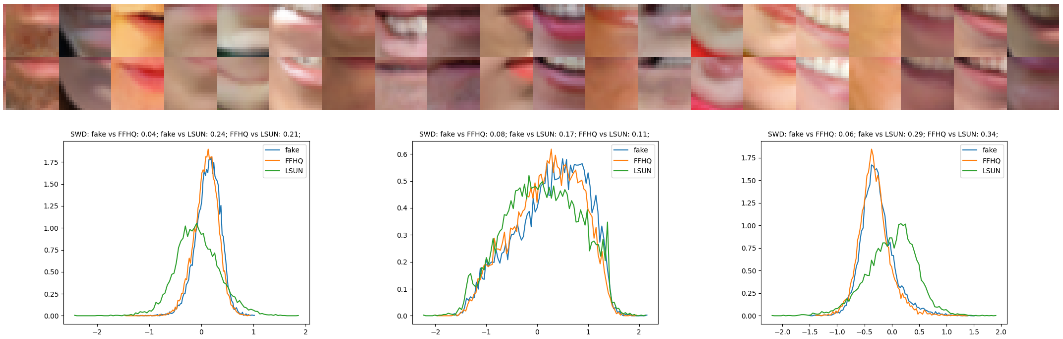

Figure 8: Top column: 20 randomly selected fake patches from a single location from a discrete GAN with $M = N = 70K$. Second column: the most similar true patches from the same location in the training set. Even though the generator never has direct access to the training images, it does a good job of copying the training patches. The mean cosine distance to the nearest neighbor is 0.99. Bottom: comparisons of histograms of random projections of fake and true patches at the same location. The histograms are almost perfectly aligned. The histogram of LSUNS patches at the same location are shown for comparison.

look very different. For example, in the MNIST data, using a CNN-GAP discriminator causes the WGAN to generate sharp digit parts, but the parts do not fit together to form a coherent digit. When we use a CNN-FC discriminator, the parts need to appear in the correct location (e.g. the top of a ”9” always appears in the top half of the generated image, not on the bottom) but the generated digits may still lack global coherence (e.g. the bottom-rightmost generated digit). In order to directly optimize patch W_1 we can no longer use OT-means because the generated patches must satisfy the constraint that they are taken from M images *with overlap*. As an alternative, we use SGD to train the same generator network used by the discrete GANs but replace the WGAN training loss with an estimate of the appropriate patch W_1.

As mentioned in the introduction we use the discrete generators to avoid using minibatch-based empirical estimates of W_1. For image W_1 we need to compute an optimal transport between $M = 64$ generated images and N training images and this is still feasible but for global patch W_1 we need to compute optimal transport between all patches in 64 images and all patches in the training images and this is infeasible. We therefore used Sliced Wasserstein distance (SWD) Pitie et al. (2005); Rabin et al. (2011); Bonneel et al. (2015) as a cheaper proxy.

The sliced Wasserstein distance is defined as the expected W_1 value between 1-d projections of two distributions into random directions. An unbiased approximation of this distance is computed from k random directions. The efficiency of SWD stems from the fact that for one dimensional data, the W_1 can be computed by simply sorting the samples and so the distance between two samples of size M can be computed in $O(M \log M)$. While in general $SWD(P, Q)$ and $W1(P, Q)$ may be different, SWD shares with W_1 the property that $SWD(P, Q) = 0$ if and only if $P = Q$. Thus by minimizing patch SWD we are encouraging the patch distribution in the fake images to match the patch distributions in the true images.

Figure 7 (2nd and 4th columns from the left) shows the results of direct optimization of patch SWD on the same datasets and using the values of M. Unlike the OT-means results, matching patch distributions yields images that preserve high frequency details and lack global structure. Clearly, discrete GANs that use convolutional discriminators generate images similar to those obtained by approximately minimizing patch distributions, not by minimizing image W_1.

Not only are the results of discrete GANs with convolutional discriminators visually similar to direct optimization, the patch SWD that they obtain is similar. For example, in the FFHQ thumbnails, the discrete GAN achieves local SWD of 0.05 direct optimization achieves local SWD of 0.03 while a random generator achieves local SWD above 0.25. Recall that $SWD = 0$ if and only if the two distributions match so this is numerical evidence that the discrete GAN is doing a good job of matching the local statistics.

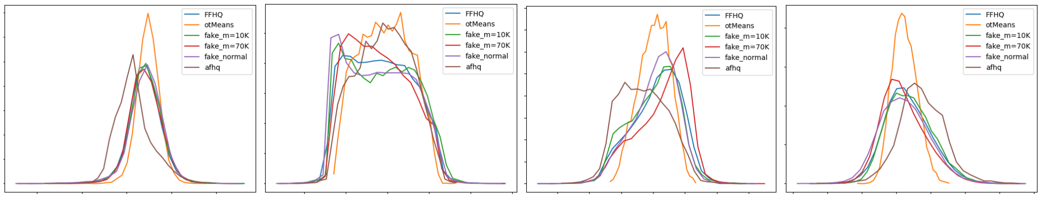

Figure 9: Evidence that the discrete DCGAN (2 leftmost plots) and FastGAN (2 rightmost plots) is matching the local statistics in the generated image and the training images. Even though each individual image is quite far from a training image, the local histograms of random projections of patches from the true images and the generated images are almost identical.This is true for various values of M including a continuous prior.

To summarize, our proofs show that theoretically WGANs with convolutional discriminators should minimize patch W_1 and not image W_1 and our experiments with toy data shows that this is indeed the case, even if we use iterative gradient training. We now ask, can the minimization of patch W_1 explain the success of WGANs in realistic datasets?

4 DO SUCCESSFUL DISCRETE GANS MINIMIZE PATCH WASSERSTEIN DISTANCE?

	Local patch swd
DCGAN m=10K	0.044
DCGAN m=70K	0.040
DCGAN m=∞	0.058
FastGAN m=10K	0.056
FastGAN m=70K	0.045
FastGAN m=∞	0.033
OTMeans = 10K	0.099
AFHQ	0.145
Imagenet	0.181

Table 1: The local SWD between true FFHQ image patches and fake image patches for different successful WGANs (averaged over locations). In all cases, the average local SWD is below 0.05. For comparison, the average local SWD between OTmeans (M=10K) patches and true FFHQ patches is around 0.1 while the average local SWD between ImageNet and FFHQ is around 0.18.

We trained discrete versions of FastGAN and DCGAN on $N = 70,000$ FFHQ images of size 128×128. We varied the number of fixed noise vectors M and found that for both architectures, the discrete GANs generate comparable results to the continuous counterparts (figures 2,4). See also figure 13 in the appendix.

The preceding theory and experiments have told us what to expect if these successful discrete GANs are minimizing Wasserstein distance. The easiest case is when $M = N$. For such a case, we expect a discrete GAN to copy images from the training set if it is minimizing image W_1 and to copy patches from the training set if it is minimizing patch W_1. Figure 8 (top) shows fake patches from a single location generated by the discrete FastGAN from figure 2 and the bottom row shows the closest match from the same location in the training set. Even though the generator never has direct access to the training images, it does a good job of copying the training patches. The mean cosine distance to the nearest neighbor is 0.99.

If the discrete GAN is minimizing patch W_1 it is not enough for it to copy patches from the training set: it should also maintain the same patch distribution. Consider for example a location where there are only two possible patches in the training set: 60% are blue patches and 40% are green patches. If the fake patches are 99% blue and 1% green, then the patch W_1 would still be high (Elnekave & Weiss, 2022). Only if the fake patches were also 60% blue and 40% green is the patch W_1 minimal. To visualize how well the discrete GAN matches the local patch distribution we considered histograms of random projections of the patches. As can be seen in three plots at the bottom of figure 8 the histograms for fake patches and true patches are almost perfectly aligned. Thus the discrete GAN is not only copying patches but also matching the local patch distribution. Even when we consider the histograms corresponding to patches in the edges of the image for true and fake images, the two histograms align quite well (see figure 12 in the appendix). Thus even for locations that often correspond to the background, the discrete GAN is matching the local patch distribution in the true and fake images.

When $M < N$ then we cannot expect the discrete GANs to copy training patches but rather its output should look like the output of OT-means on patches from a single location (see appendix C): each generated patch is a linear combination of training patches and the local histograms of true and fake patches at a location should match. Figure 9 shows that the local distribution is matched very well for a discrete DCGAN with different values of M. Importantly, the matching also holds with the continuous prior.

We summarize all of our experiments in table 1: for the two GAN architectures and for different values of M, the local distributions at a particular location are well matched between the true images and the generated images. As a reference we also compute the distance to a batches of 10K images from ImageNet and from AFHQ (Choi et al., 2020): the average local SWD between AFHQ and FFHQ is about 0.15 and 0.18 while the different WGANs consistently achieve a local SWD that is about 0.04.

5 LIMITATIONS AND EXTENSIONS

Our theoretical results are based on simplifications of convolutional discriminators used in practice. One major simplification is that we assume that the receptive field sizes are at most S and this value of S determines the patch size used in patch W_1. For practical CNNs, the theoretical limit on the receptive field may be very large, but the effective receptive field size is still small (Brendel & Bethge, 2019) and the CNN can be well-approximated as if the receptive field size was much smaller than the theoretical limit. A second simplification is that we implicitly assumed that the CNNs do not use any padding when performing convolutions (and this was also the case in the GANs that we trained for the toy data). When padding is used, patches at different image locations can actually be distinguished even with a patch-based discriminator (e.g. (Isola et al., 2017),(Shaham et al., 2019)) so even a CNN-GAP discriminator will optimize a patch distance that is location-dependent.

Even though our use of the discrete setting allows us to exactly measure W_1 between true and fake images, it still leaves open the question of how small W_1 needs to be in order for a method to be described as ”successful” in minimizing W_1. For this reason, we compare the results of the WGANs to direct optimization of W_1 and also visualize the histograms and measure their distance using SWD.

The most significant limitation of our paper, of course, is our focus on discrete GANs while SOTA GANs use a continuous prior. We note that most of our theoretical results do not require the GANs to be discrete: working with discrete GANs allows us to empirically measure W_1 and to rigorously determine whether the predictions hold. In practice, we find that continuous GANs with convolutional discriminators behave similarly to their discrete counterparts (with large M).

6 DISCUSSION

The question that motivated this paper is whether WGANs suceeed because they optimize the Wasserstein distance. We leveraged the discrete setting that allows us to compute the Wasserstein distance exactly, to characterize its optima and to optimize it with alternative algorithms. Our results indicate that the answer is ”yes” but the form of W_1 that is being optimized depends on the architecture of the discriminator. Specifically we have shown that when the discriminator is convolutional, what is being minimized is the patch W_1 and not the image W_1.

A major advantage of having a well-defined loss function that is being optimized is the ability to monitor learning algorithms and check for their convergence. We hope that our results will yield WGAN learning algorithms that are considerably more stable than the current methods and require less parameter tuning.

REFERENCES

Cem Anil, James Lucas, and Roger Grosse. Sorting out Lipschitz function approximation. In Kamalika Chaudhuri and Ruslan Salakhutdinov (eds.), *Proceedings of the 36th International Conference on Machine Learning*, volume 97 of *Proceedings of Machine Learning Research*, pp. 291–301. PMLR, 09–15 Jun 2019. URL `https://proceedings.mlr.press/v97/anil19a.html`.

Martin Arjovsky, Soumith Chintala, and Léon Bottou. Wasserstein generative adversarial networks. In *International conference on machine learning*, pp. 214–223. PMLR, 2017.

Nicolas Bonneel, Julien Rabin, Gabriel Peyré, and Hanspeter Pfister. Sliced and radon wasserstein barycenters of measures. *Journal of Mathematical Imaging and Vision*, 51(1):22–45, 2015.

Wieland Brendel and Matthias Bethge. Approximating cnns with bag-of-local-features models works surprisingly well on imagenet. *arXiv preprint arXiv:1904.00760*, 2019.

Andrew Brock, Jeff Donahue, and Karen Simonyan. Large scale gan training for high fidelity natural image synthesis. *arXiv preprint arXiv:1809.11096*, 2018.

Yunjey Choi, Youngjung Uh, Jaejun Yoo, and Jung-Woo Ha. Stargan v2: Diverse image synthesis for multiple domains. In *Proceedings of the IEEE/CVF conference on computer vision and pattern recognition*, pp. 8188–8197, 2020.

Ariel Elnekave and Yair Weiss. Generating natural images with direct patch distributions matching. In *European Conference on Computer Vision*, pp. 544–560. Springer, 2022.

Farzan Farnia and Asuman Ozdaglar. Do gans always have nash equilibria? In *International Conference on Machine Learning*, pp. 3029–3039. PMLR, 2020.

William Fedus, Mihaela Rosca, Balaji Lakshminarayanan, Andrew M Dai, Shakir Mohamed, and Ian Goodfellow. Many paths to equilibrium: Gans do not need to decrease a divergence at every step. *arXiv preprint arXiv:1710.08446*, 2017.

William Fedus, Mihaela Rosca, Balaji Lakshminarayanan, Andrew M Dai, Shakir Mohamed, and Ian Goodfellow. Many paths to equilibrium: Gans do not need to decrease a divergence at every step. In *International Conference on Learning Representations*, 2018.

Ian Goodfellow, Jean Pouget-Abadie, Mehdi Mirza, Bing Xu, David Warde-Farley, Sherjil Ozair, Aaron Courville, and Yoshua Bengio. Generative adversarial networks. *Communications of the ACM*, 63(11):139–144, 2020.

Ishaan Gulrajani, Faruk Ahmed, Martin Arjovsky, Vincent Dumoulin, and Aaron C Courville. Improved training of wasserstein gans. *Advances in neural information processing systems*, 30, 2017.

Kurt Hornik, Maxwell Stinchcombe, and Halbert White. Multilayer feedforward networks are universal approximators. *Neural networks*, 2(5):359–366, 1989.

Phillip Isola, Jun-Yan Zhu, Tinghui Zhou, and Alexei A Efros. Image-to-image translation with conditional adversarial networks. In *Proceedings of the IEEE conference on computer vision and pattern recognition*, pp. 1125–1134, 2017.

Tero Karras, Samuli Laine, Miika Aittala, Janne Hellsten, Jaakko Lehtinen, and Timo Aila. Analyzing and improving the image quality of stylegan. In *Proceedings of the IEEE/CVF conference on computer vision and pattern recognition*, pp. 8110–8119, 2020.

Alexander Korotin, Lingxiao Li, Aude Genevay, Justin M Solomon, Alexander Filippov, and Evgeny Burnaev. Do neural optimal transport solvers work? a continuous wasserstein-2 benchmark. *Advances in Neural Information Processing Systems*, 34:14593–14605, 2021.

Alexander Korotin, Alexander Kolesov, and Evgeny Burnaev. Kantorovich strikes back! wasserstein gans are not optimal transport? *Advances in Neural Information Processing Systems*, 35:13933–13946, 2022.

Bingchen Liu, Yizhe Zhu, Kunpeng Song, and Ahmed Elgammal. Towards faster and stabilized gan training for high-fidelity few-shot image synthesis. In *International Conference on Learning Representations*, 2020.

Anton Mallasto, Guido Montúfar, and Augusto Gerolin. How well do wgans estimate the wasserstein metric? *arXiv preprint arXiv:1910.03875*, 2019.

Tristan Milne and Adrian I Nachman. Wasserstein gans with gradient penalty compute congested transport. In *Conference on Learning Theory*, pp. 103–129. PMLR, 2022.

Takeru Miyato, Toshiki Kataoka, Masanori Koyama, and Yuichi Yoshida. Spectral normalization for generative adversarial networks. *arXiv preprint arXiv:1802.05957*, 2018.

Xingang Pan, Ayush Tewari, Thomas Leimkühler, Lingjie Liu, Abhimitra Meka, and Christian Theobalt. Drag your gan: Interactive point-based manipulation on the generative image manifold. In *ACM SIGGRAPH 2023 Conference Proceedings*, pp. 1–11, 2023.

Thomas Pinetz, Daniel Soukup, and Thomas Pock. On the estimation of the wasserstein distance in generative models. In *Pattern Recognition: 41st DAGM German Conference, DAGM GCPR 2019, Dortmund, Germany, September 10–13, 2019, Proceedings 41*, pp. 156–170. Springer, 2019.

Francois Pitie, Anil C Kokaram, and Rozenn Dahyot. N-dimensional probability density function transfer and its application to color transfer. In *Tenth IEEE International Conference on Computer Vision (ICCV'05) Volume 1*, volume 2, pp. 1434–1439. IEEE, 2005.

Chongli Qin, Yan Wu, Jost Tobias Springenberg, Andy Brock, Jeff Donahue, Timothy Lillicrap, and Pushmeet Kohli. Training generative adversarial networks by solving ordinary differential equations. *Advances in Neural Information Processing Systems*, 33:5599–5609, 2020.

Julien Rabin, Gabriel Peyré, Julie Delon, and Marc Bernot. Wasserstein barycenter and its application to texture mixing. In *International Conference on Scale Space and Variational Methods in Computer Vision*, pp. 435–446. Springer, 2011.

Alec Radford, Luke Metz, and Soumith Chintala. Unsupervised representation learning with deep convolutional generative adversarial networks. *arXiv preprint arXiv:1511.06434*, 2015.

Axel Sauer, Katja Schwarz, and Andreas Geiger. Stylegan-xl: Scaling stylegan to large diverse datasets. In *ACM SIGGRAPH 2022 conference proceedings*, pp. 1–10, 2022.

Florian Schäfer, Hongkai Zheng, and Anima Anandkumar. Implicit competitive regularization in gans. *arXiv preprint arXiv:1910.05852*, 2019.

Tamar Rott Shaham, Tali Dekel, and Tomer Michaeli. Singan: Learning a generative model from a single natural image. In *Proceedings of the IEEE/CVF international conference on computer vision*, pp. 4570–4580, 2019.

Sahil Sidheekh, Aroof Aimen, and Narayanan C Krishnan. On characterizing gan convergence through proximal duality gap. In *International Conference on Machine Learning*, pp. 9660–9670. PMLR, 2021.

Jan Stanczuk, Christian Etmann, Lisa Maria Kreusser, and Carola-Bibiane Schönlieb. Wasserstein gans work because they fail (to approximate the wasserstein distance). *arXiv preprint arXiv:2103.01678*, 2021.

Jonathan Weed and Francis Bach. Sharp asymptotic and finite-sample rates of convergence of empirical measures in wasserstein distance. 2019.

Endre Weiszfeld. Sur le point pour lequel la somme des distances de n points donnés est minimum. *Tohoku Mathematical Journal, First Series*, 43:355–386, 1937.

A PROOFS

A.1 PROOF OF THEOREM 2.4

To show that for $M < N$ at any local minimum the generator must be a linear combination of at least N/M training examples, we differentiate equation 3 with respect to a generated image x_i and setting the gradient to zero yields that x_i must satisfy:

$$x_i = \sum_j w_{ij} y_j$$

with w_{ij} a vector of weights that sums to one and $w_{ij} \propto \pi_{ij} \|x_j - y_i\|^{-1}$. Now since π_{ij} is a solution to the optimal transport between M generated images and N training images, it is a non-negative matrix that satisfies $\sum_i \pi_{ij} = \frac{1}{N}$ and $\sum_j \pi_{ij} = \frac{1}{M}$. This implies that for each i there must be at least N/M different indices j for which $\pi_{ij} > 0$ and this shows that y must be a linear combination of at least N/M training images.

A.2 PROOF OF THEOREM 3.3

We can write the output of the critic for an input x as:

$$f(x) = W^T \frac{1}{n} \sum_i h(p_i x)$$

where $p_i x$ extracts the ith patch in image x, W are the weights in the final layer, and n is the number of patches in the penultimate feature map.

Moving W^T into the above sum and defining $g(x) = W^T h(x)$ where x is a patch we can rewrite the image critic, $f(x)$ as:

$$f(x) = \frac{1}{n} \sum_i g(P_i x)$$

Recall that the critic f attempts to maximize $E_P(f) - E_Q(f)$. By the linearity of the expectation $E_Q(f)$ is equal to $E_{\tilde{Q}}(g)$ and likewise $E_{P_\theta}(f) = E_{\tilde{P}_\theta}(g)$ where $\tilde{P}, \tilde{Q}$ are the distributions over patches in the true and fake images. Denoting by GAP_1 the class of 1-Lipshitz functions that can be implemented by a CNN-GAP architecture, this means that:

$$\underset{f \in GAP_1}{max} E_{P_\theta}(f) - E_Q(f) = \max_{g \in G_1} E_{\tilde{P}_\theta}(g) - E_{\tilde{Q}}(g)$$

G_1 is the class of functions that operate on $S \times S$ patches and can be implemented by the units in the layer before the GAP.

A.3 PROOF OF THEOREM 3.4

We can write the output of the critic for an input x as:

$$f(x) = \sum_c \sum_i w_{ic} f_c(P_i x) \tag{4}$$

where $P_i x$ extracts the ith patch in image x, C is the number of channels and w_{ic} the weights in the final layer.

Now define the function class CNN as all functions that can be implemented using equation 4 and the subclass CNN_k as the set of functions that can be implemented by equation 4 where $w_{jc} = 0$ $\forall c$, $\forall j \neq k$. Since $CNN_i \subset CNN$ we have

$$\max_{f \in CNN} E_{P_\theta}(f) - E_Q(f) \geq \max_{f \in CNN_i} E_{P_\theta}(f) - E_Q(f)$$

and since for $f \in CNN_i$ f is only a function of the ith patch we can write:

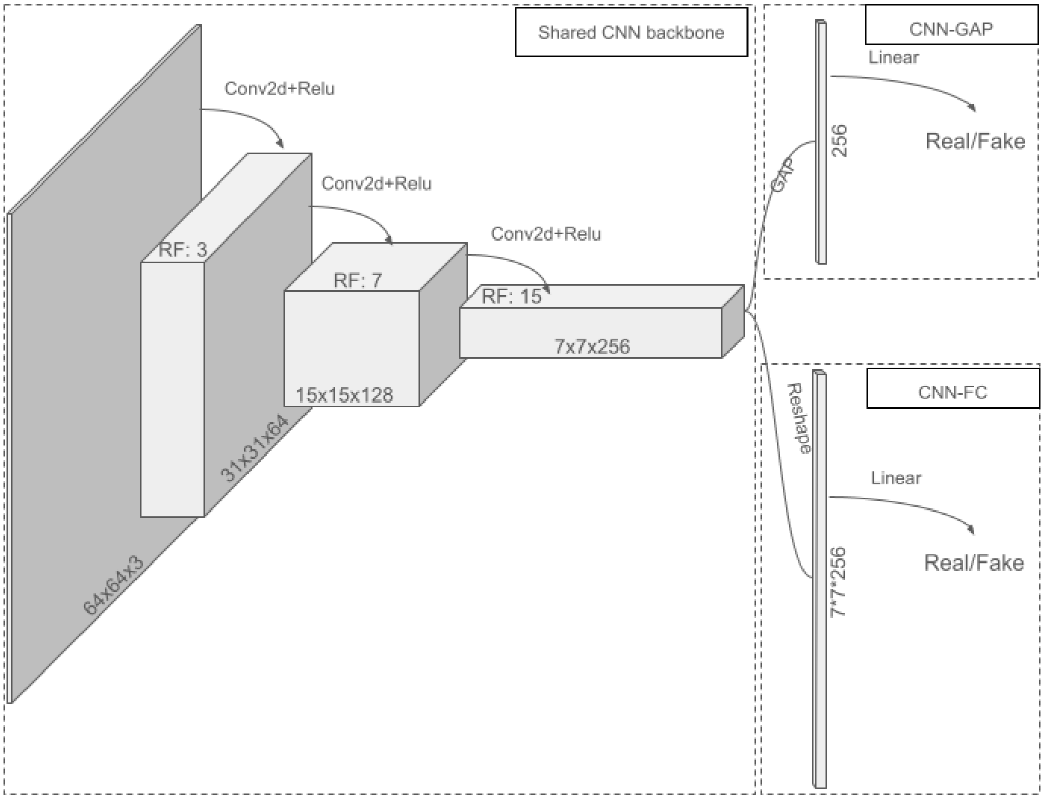

Figure 10: An illustration of the toy CNN used the experiments in figures 5-7. 3 Convolutional layers are followed by two type of linear heads that project the feature map into a scalar. The annotation **RF** stands for the receptive field of the previous layer.

$$\begin{aligned}\max_{f\in CNN_i} E_{P_\theta}(f) - E_Q(f) &= \max_{i\in I, g_i\in G} E_{\tilde{P}_\theta}(g_i) - E_{\tilde{Q}}(g_i) \\ &= \max_{i\in I} W_1^{patches_i}(P_\theta, Q)\end{aligned}$$

where again $g_i(x)$ is a critic for the ith patch: $g_i(x) = \sum_c w_{ic} f_c(P_i x)$.

B ARCHITECTURES

B.1 TOY CNNS

We bring here further details about CNN-GAP and CNN-FC architectures used in the the experiment section. Both architectures start with 3 convolutional layers with kernel size 3, stride 2 and no padding each followed by a RELU layer. These layers transform an 64x64x3 image to a 7x7x256 features map. The receptive field at this point, i.e, the size of the patch in the original images that affect each pixel in this feature map is 15x15. CNN-GAP applies global average pooling to this feature map that transforms it into a 1x1x256 layer that is later linearly projected into a scalar. CNN-FC reshapes the feature map into a long vector of 7*7*256 that is linearly projected into a scalar. Figure 10 illustrates the two architecture with their common backbone.

B.2 FASTGAN VARIANT

We experimented with FastGAN Liu et al. (2020) as an easy, fast to converge GAN model that performs comparably to SOTA GANs. In our experiments we simplified its architecture branching

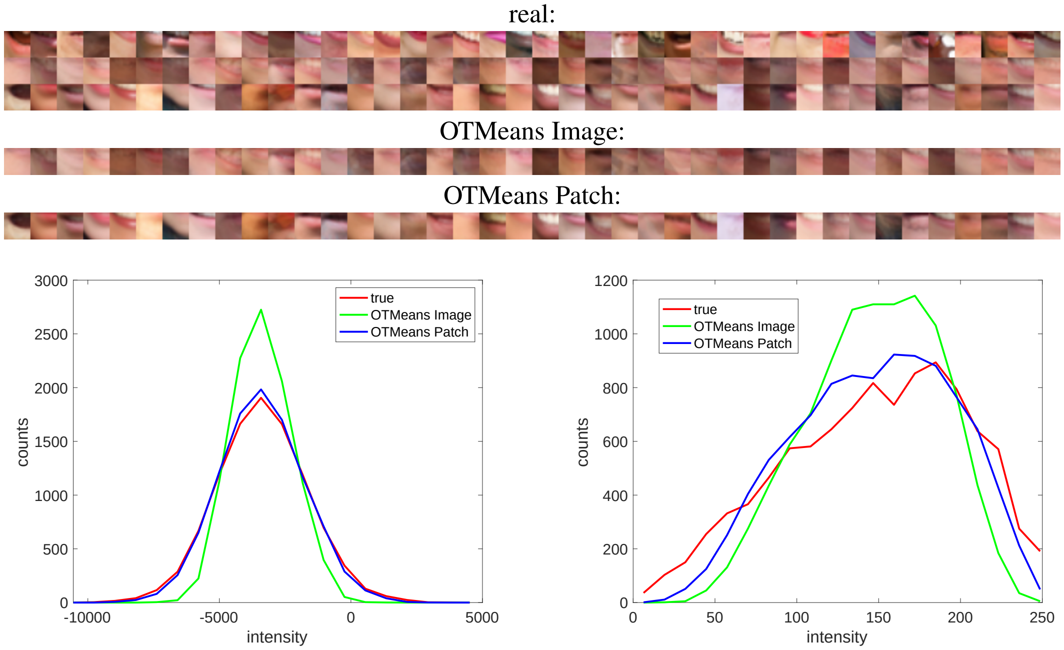

Figure 11: The difference between minimizing image W_1 and patch W_1. When we minimize image W_1 and then extract small (20×20) patches (middle row) the extracted patches look very different from the training patches. When we minimize patch W_1, i.e. the Wasserstein distance between 20×20 patches at that location in the true and fake images, the generated patches (bottom row) look similar to real patches. The success in capturing the local patch distribution can be visualized by comparing the histograms of random projections of the patches.

off this implementation [2]. We removed the auto-encodeing brances of the discriminator so that both the generator and the discriminator are simple feed-forward networks with skip connections.

C OTMEANS ON PATCHES

One reason to expect better results with the minimization of patch W_1 is related to theorem 2.4: minimizing image W_1 causes the generator to either copy the training set or to generate images that are linear combinations of several training images and will therefore be of poor visual quality. But if we minimize patch W_1 we can still generate images that are very different from the training images by copying patches from the training set and combining them in novel ways. We can also generate patches that are linear combination of training patches, but since the distribution of patches is simpler in some sense than that of images, linear combinations of training patches do not necessarily have to be blurred. Figure 11 illustrates this point. We minimized patch W_1 by running OTmeans with $M = 10,000$ only on a small 20x20 patch in a location that corresponds to the left part of the mouth. We then compared the generated patches to those obtained by running OTmeans on the full image (hence minimizing image W_1) and then extracting the patches. As can be seen in the figure, the patches obtained by minimizing patch W_1 are high-contrast and sharp, unlike the patches obtained by minimizing image W_1.

We can visualize how well the generated patches match the distribution of training patches by plotting the histogram of random projections of the patches. As shown in the bottom of figure 11, when we minimize image W_1 the histograms of projections of generated patches are visibly different from those of training patches at the same location. When we minimize the local patch W_1, the histograms match very well.

---

[2] https://github.com/odegeasslbc/FastGAN-pytorch/blob/main/models.py

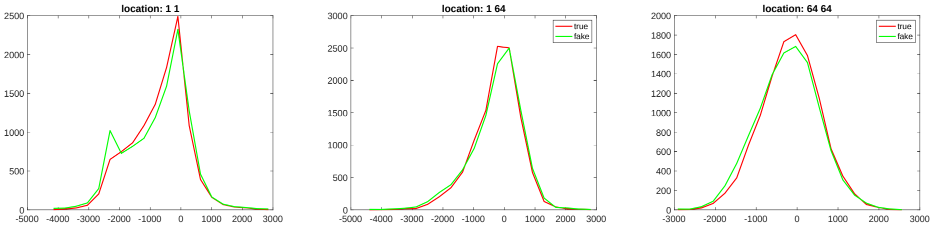

Figure 12: Histograms of the same random projection for true and fake patches at different locations. Note that the histograms are different between different locations but highly similar for true and fake patches. This is true even for locations at the edge of the image.

D HISTOGRAMS AT DIFFERENT LOCATIONS

Figure 12 visualize how well the discrete GAN matches the local patch distribution we considered histograms of random projections of the patches in additional 3 locations.

E RESULTS WITH DISCRETE SOTA ARCHITECTURES

We bring here the results of training discrete-WGANs with more capable architectures. As can be seen, for both DCGAN Radford et al. (2015) and FastGAN Liu et al. (2020) the results with two different discrete priors (M=10K,70K) are comparable to the results with normal prior ($M=\infty$). Each second row shows the data nearest neighbor to show there is not copying involved.

E.1 RESULTS WITH DISCRETE DCGAN

See generated images and data nearest neighbors in figure 13

E.2 RESULTS WITH DISCRETE FASTGAN

See generated images and data nearest neighbors in figure 14

F ADDITIONAL ABLATION EXPERIMENTS FOR REVIEWERS

F.1 RESULTS WITH CONVOLUTIONAL GENERATOR

In all of the experiments in the paper we used the same FC generator. We Repeat here the results from figures 5 and 8 from the paper with a convolutional generator (DCGANRadford et al. (2015). As can be seen in figure 15 the WGAN and direct optimization show similar behavior.

F.2 RESULTS WITH DIFFERENT GAN LOSSES

Our paper deals with WGANs. While the same can be done for all IPMs like Sobolev GANs and MMD GANs it may not be directly applied to some other losses like the original or non-saturating GAN losses. However, our experiments with Non-saturating GANs show (figure 16) similar results.

F.3 RESULTS WITH DIFFERENT PATCH SIZES

We have conducted experiments from figures 5,7 with different patch sizes. We used less convolutional layers in the discriminator to get patch size=8 and the same number of layers (3) with kernel size 4 (instead of 3) to get a patch size of 22. As can be seen in figure 17 observed that the relevant patch size indeed changes as predicted. This figure compares WGANs trained with CNN-GAP discriminators of different depth and thus different receptive fields. As can be seen, with a shallow discriminator the generated images preserve statistics of smaller patches. We will discuss these results in the final version.

$M = 10,000$:

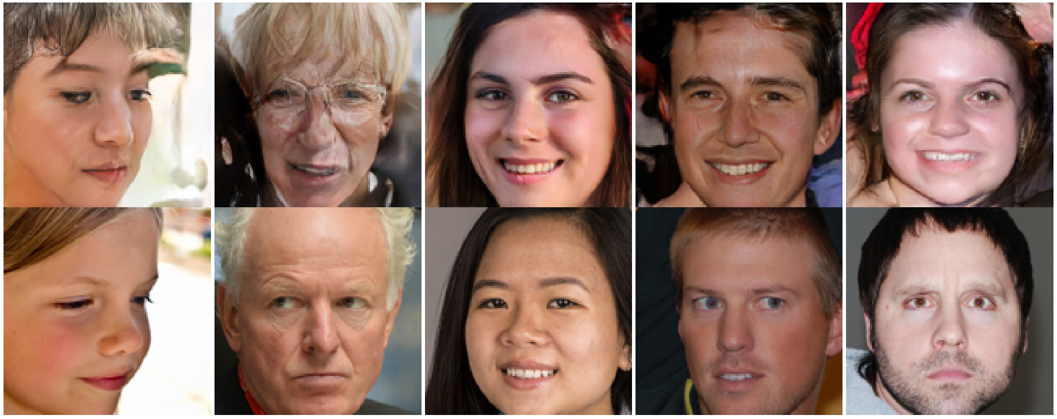

$M = 70,000$:

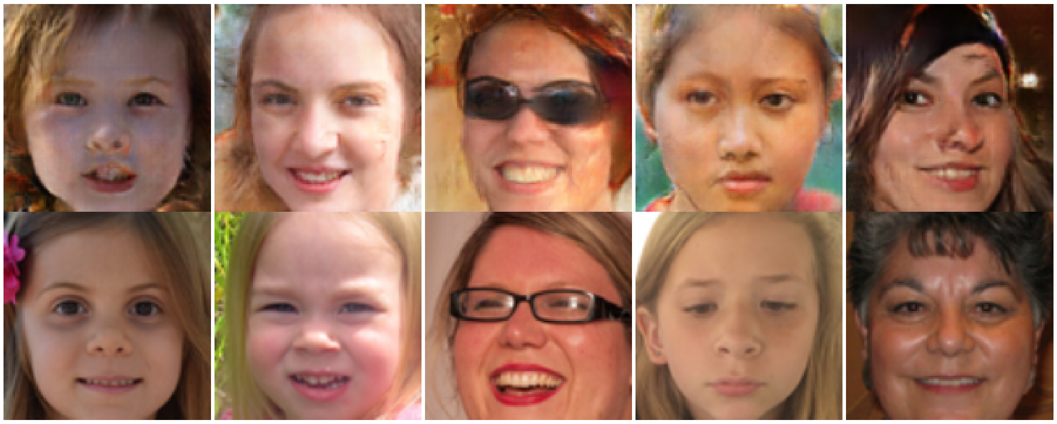

$M = \infty$:

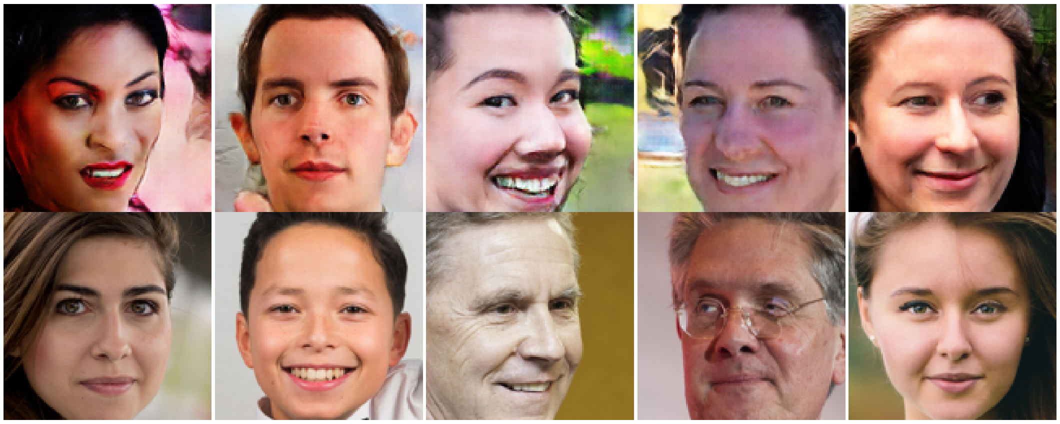

Figure 13: Images generated with Discrete DCGAN for different values of M. For each value of M we show five generated images and below them the closest image from the training set for each generated image.

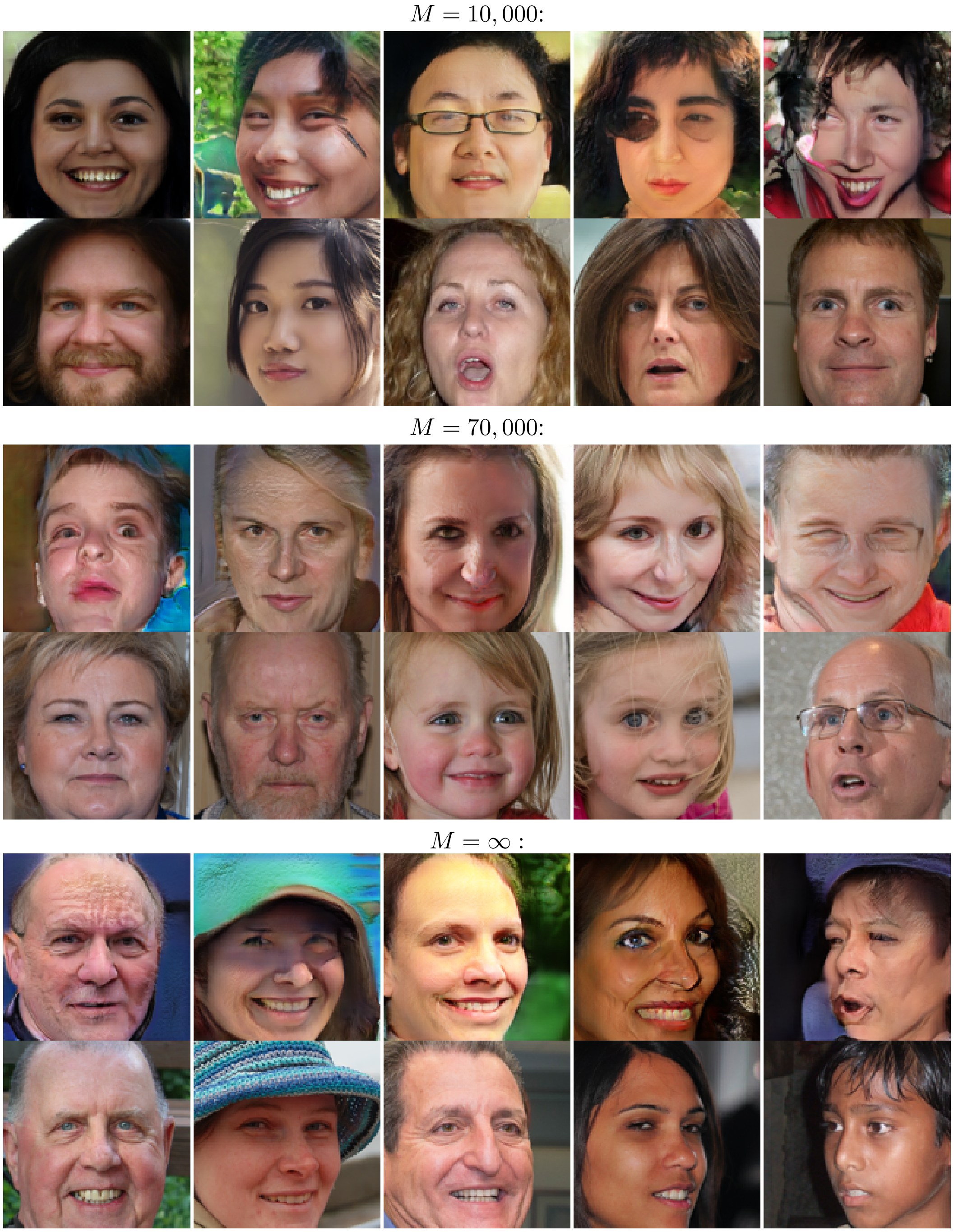

$M = 10,000$:

$M = 70,000$:

$M = \infty$:

Figure 14: Images generated with Discrete FastGAN variant for different values of M. For each value of M we show five generated images and below them the closest image from the training set for each generated image.

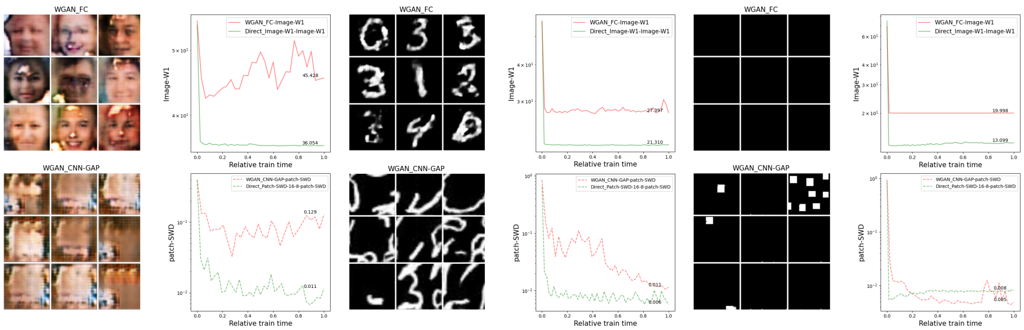

(a) FFHQ (b) Mnist (c) Squares

Figure 15: Comparing direct optimization in image/patch level with WGAN with FC/Convolutional discriminator when the generator is convolutional

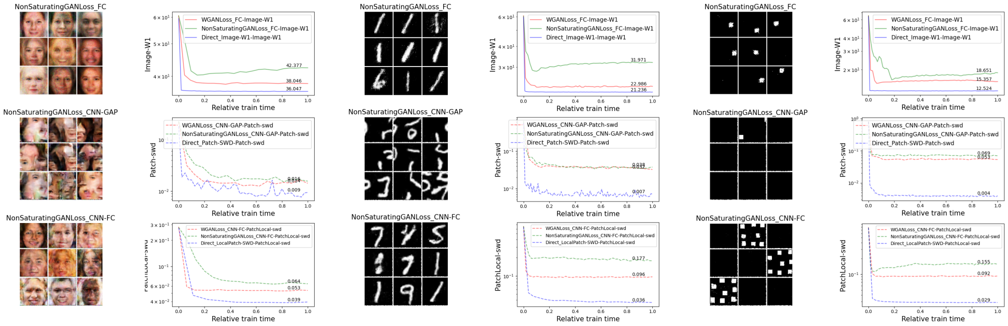

(a) FFHQ (b) Mnist (c) Squares

Figure 16: Results of training NS-GAN with FC/Convolutional discriminators. As can be seen, we see the same trend as with WGAN where the discriminator architecture controls whether the statistic being preserved is in the image or the patch level. The graphs also show metrics taken from the same model trained with WGAN loss and of a direct optimization for reference.

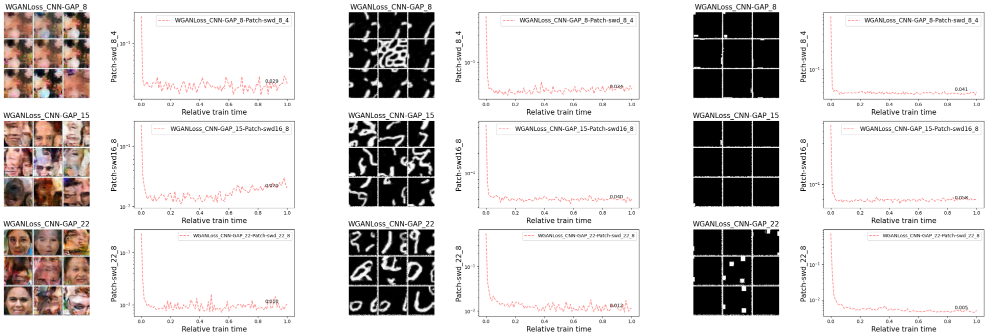

(a) FFHQ (b) Mnist (c) Squares

Figure 17: Results of WGAN trained with with FC/Convolutional discriminator when in different patch sizes. As can be seen, as the patch size grows the statistics of bigger patches is preserved.

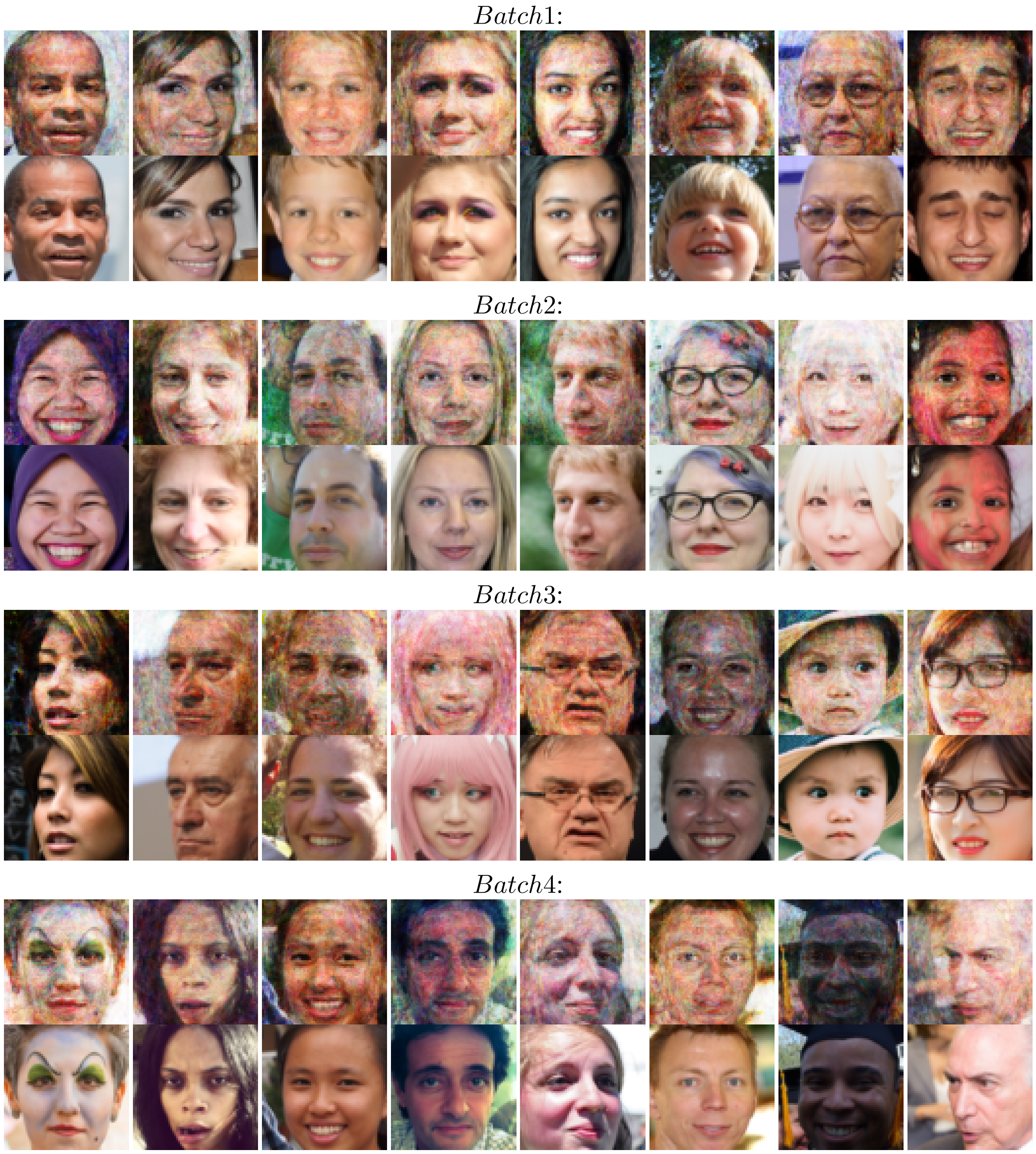

Figure 18: Additional 4 batches of results from the model from figure 6 trained with M=N=1K on FFHQ each batch's top row shows fake images and the bottom row shows data nearest neighbors.

F.4 ADDITIONAL RESULTS WITH M=N

We bring here in figure 18 more results from the experiment of figure 6